Integration of proteomic and genetic approaches to assess developmental muscle atrophy

David S. Brooks[1†], Kumar Vishal[1,2†], Simranjot Bawa[1], Adrienne Alder[1], and Erika R. Geisbrecht[1*]

[1] Department of Biochemistry and Molecular Biophysics, Kansas State University, Manhattan, Kansas 66506

[2]Current address: Shiley BioScience Center, San Diego State University, San Diego, CA, 92182

[†] Contributed equally as first authors

*Corresponding author

E-mail: geisbrechte@ksu.edu

SUMMARY STATEMENT

An evolutionarily conserved set of proteins are essential for muscle atrophy in the *Drosophila* and *Manduca* insect models.

ABSTRACT

Muscle atrophy, or a decline in muscle protein mass, is a significant problem in the aging population and in numerous disease states. Unraveling molecular signals that trigger and promote atrophy may lead to a better understanding of treatment options; however, there is no single cause of atrophy identified to date. To gain insight into this problem, we chose to investigate changes in protein profiles during muscle atrophy in *Manduca sexta* and *Drosophila melanogaster*. The use of insect models provides an

interesting parallel to probe atrophic mechanisms since these organisms undergo a normal developmental atrophy process during the pupal transition stage. Leveraging the inherent advantages of each model organism, we first defined protein signature changes during *Manduca* intersegmental muscle (ISM) atrophy and then used genetic approaches to confirm their functional importance in the *Drosophila* dorsal internal oblique muscles (DIOMs). Our data reveal an upregulation of proteasome and peptidase components and a general downregulation of proteins that regulate actin filament formation. Surprisingly, thick filament proteins that comprise the A band are increased in abundance, providing support for the ordered destruction of myofibrillar components during developmental atrophy. We also uncover the actin filament regulator Ciboulot (Cib) as a novel regulator of muscle atrophy. These insights provide a framework towards a better understanding of global changes that occur during atrophy and may lead to eventual therapeutic targets.

INTRODUCTION

The inadequate maintenance of muscle tissue mass, or muscle atrophy, has severe consequences in maintaining normal life activities and is a contributing factor to increased morbidity rates (Bonaldo and Sandri, 2013; Ebert et al., 2019; Piccirillo et al., 2014). In humans, progressive muscle wasting due to advanced disease states (e.g., cancer, diabetes, etc.) or aging decreases quality of life, limits economic opportunities for living wages, and increases healthcare costs. While many studies have examined the triggers and resulting physiological changes associated with muscle wasting, details concerning the molecular basis of these diseases are only emerging. A better understanding of the mechanisms that contribute to muscle wasting must first be established before successful therapeutic strategies can be developed.

Numerous mouse models exist that mimic muscle disuse or disease states predicted to recapitulate atrophic conditions. Examples include mechanical ventilation to induce diaphragm atrophy, limb immobilization, hind-limb suspension, denervation, and exposure to high doses of glucocorticoids (Gao et al., 2018; Malavaki et al., 2015; Romanick et al., 2013). These steroid hormones are released in times of stress as a result of renal failure, diabetes, or sepsis and result in muscle atrophy by inhibiting amino acid

import and protein synthesis (Braun and Marks, 2015; Schakman et al., 2013). Because glucocorticoids reduce inflammation in the treatment of autoimmune diseases, arthritis, and cancer, muscle wasting is an adverse side effect of prolonged treatment. Unfortunately, complex interactions between multiple tissues and the infiltration of immune cells that promote inflammation and drive disease progression prevent a complete understanding of the muscle autonomous contribution to muscle wasting.

The normal histolysis of muscles that occurs during insect pupal development provides a unique opportunity to study muscle intrinsic properties that contribute to a reduction in muscle mass while maintaining contractile strength (Piccirillo et al., 2014; Schwartz, 2008; Schwartz, 2018). Studying this stereotyped developmental atrophy has several inherent advantages. First, the time course is shorter in insect models, whereby atrophy is accomplished in hours or a few days compared to weeks for mammalian induced atrophy models. Second, developmental atrophy is not lethal, which allows for observation of the complete atrophy process in addition to dissecting factors that contribute to atrophy initiation versus progression. Third, developmental atrophy is induced by a class of insect steroid hormones called ecdysteroids (Schwartz and Truman, 1983; Zirin et al., 2013). The rapid loss of muscle mass caused by the structurally related glucocorticoids and ecdysteroids suggest similar mechanisms of action that may identify mechanisms common to multiple types of induced atrophies. Finally, the set of genetic and biochemical tools available in insect models is extensive, allowing for spatial and temporal control to manipulate gene function and an arsenal of RNAi lines for tissue-specific knockdown.

Herein we utilize the capabilities of two insect models, the tobacco hornworm moth *Manduca sexta* and the fruit fly *Drosophila melanogaster,* to uncover and characterize novel proteins essential for developmental muscle atrophy. Each organism is beneficial for different reasons. The large size of *Manduca* make it an ideal biochemical model to uncover novel proteins that are upregulated or downregulated during muscle atrophy, while the functional requirement for these genes is confirmed in the *in vivo* platform afforded through *Drosophila* genetics. Sets of muscles in both organisms undergo atrophy during pupal development. In *Manduca,* the large intersegmental muscles (ISMs) lose ~40% of their muscle mass in the three days prior to adult eclosion (Bayline

et al., 2005; Schwartz and Truman, 1983). Isolation of ISMs from a single organism provides enough material for biochemical analysis. In *Drosophila*, genetic tools exist to knockdown or overexpress genes in the dorsal internal oblique muscles (DIOMs) that undergo atrophy (Kuleesha et al., 2016a; Kuleesha et al., 2016b; Wasser et al., 2007; Zirin et al., 2013).

Multiple studies in *Manduca* have defined factors that contribute to the ISM atrophy program. The insect molting hormone 20-hydroxyecdysone (20E) triggers atrophy and prolonged administration of 20E is sufficient to block ISM degeneration and subsequent programmed cell death (Bayline et al., 2005; Schwartz and Truman, 1983). This reliance on hormone signaling strongly suggests transcriptional programs largely mediate the atrophy process. Indeed, analysis of individual mRNAs or genome-wide RNA sequencing has revealed a decline of muscle structural genes and upregulation of genes that promote proteasomal turnover (Haas et al., 1995; Schwartz et al., 1990), both of which are hallmarks of mammalian muscle atrophy (Bilodeau et al., 2016; Khalil, 2018; Kitajima et al., 2020). In *Drosophila*, inhibition of TOR signaling via RNAi knockdown of *Rheb* or *Tor* enhanced DIOM atrophy, while a reduction of the negative regulators *Tsc1* and *Tsc2* caused larger muscles that failed to undergo atrophy (Kuleesha et al., 2016a). Since Tor signaling promotes muscle growth by inhibiting autophagy, it is not too surprising that RNAi silencing *of Atg5, Atg9, Atg12, Atg17*, or *Atg18* also prevents muscle loss.

Here we expand upon these previous studies to examine changes in protein levels at the initiation (D15) or conclusion (D18) of developmental atrophy in *Manduca*. We find that proteins required for protein catabolism and energy production are globally induced. Also evident is the tight regulation of thin filament breakdown, whereby actin disassembly proteins are increased with a corresponding reduction in actin filament promoting proteins. Surprisingly, a number of thick filament proteins remain during atrophy, suggesting an ordered breakdown of myofibril components.

MATERIALS AND METHODS

Manduca collection and staging

Manduca sexta specimens were a kind gift of Dr. Mike Kanost (Department of Biochemistry and Molecular Biophysics, Kansas State University). Pupae were staged as previously described (Schwartz and Truman, 1983). Briefly, 0-1 day old male pupae were transferred to a 26^{0}C incubator and raised with a 12-hour light and 12-hour dark cycle. Samples were processed between 8 a.m. and 10 a.m. on D15 at the beginning of muscle atrophy or on D18 near the end of muscle atrophy, but before adult eclosion.

ISM sample collection and peptide identification

1D gels. During dissection of staged D15 or D18 pupae, the ISMs were removed, washed with ice-cold saline (4 mM NaCl, 40 mM KCl, 18 mM MgCl, 3 mM $CaCl_2$, 1.5 mM PIPES pH =6.5, 41.5 g sucrose in 500mL ultrapure water), transferred to separate Eppendorf tubes, flash frozen in liquid nitrogen, and stored at -80^{0}C. After thawing, samples were lysed in ~2 mL of 50 mM Tris + 1% SDS in a glass homogenizer on ice and were then centrifuged at 20,000 x g for 10 min at 4^{0}C to pellet debris. Total protein was determined using the Bicinchoninic acid (BCA) assay (Pierce). Approximately 35 µg of each sample was mixed with SDS sample reducing buffer (0.5 M Tris-HCl pH 6.8, 10% glycerol, 10% (w/v) SDS, 0.5% (w/v) bromophenol blue) and run on a 10% SDS-PAGE gel. Proteins were visualized with Coomassie Blue (3 g/L Coomassie Brilliant Blue R250, 45% methanol, 10% acetic acid) staining followed by destaining (45% methanol, 10% acetic acid). The gel was sent to the Recombinant DNA/Protein Core Facility at Oklahoma State University for mass spectrometry (MS) analysis. Independent gel lanes were fractionated and trypsinized as described (Voruganti et al., 2018). Peptides were analyzed on 75 micrometer x 40 cm nano-columns fabricated in house, and packed with 3-micron beads of Magic AQ C18 resin (Michrom). Peptides were injected using a vented trap column configuration, and separated on 6%-35% linear acetonitrile gradients developed over a 100-minute chromatography run at 250 nL/min. Columns terminated in a stainless-steel emitter for peptide ionization within a Nanospray Flex ion source (Thermo). Peptide ions were analyzed in a quadrupole-Orbitrap “Fusion” mass spectrometer (Thermo) using a 3-second “top speed” data-dependent MS/MS scan

method. In this method, peptide precursors were measured within the Orbitrap sector at a nominal resolution of 120,000. Ions were selected for MS/MS using the quadrupole, followed by collision-induced dissociation (CID) fragmentation and analysis of the fragments using the ion trap detector. Peptides from each individual adsorption sample were subjected to three individual LC-MS/MS analyses ("technical replicates"). Biological replicates were performed as indicated in Figure 1C. Peptides were identified and quantified by using MaxQuant v1.5.3.8 (Cox and Mann, 2008) to search a database of 27,403 *Manduca* sequences downloaded from https://data.nal.usda.gov/dataset/*Manduca*-sexta-official-gene-set-v20. Database searches utilized the default MaxQuant parameters.

2D gels. *Manduca* samples were prepared as described above. 100 µg of each sample was added to 2D sample buffer (8 M urea, 2% CHAPS, 0.05 M DTT, 1X Biolyte 3-10, and 0.001% bromophenol blue), transferred to separate lanes of a BioRad Protean IEF focusing tray containing ReadyStrip IPG strips, pH 5-8 or pH3-6, 7cm (BioRad), and covered with mineral oil. The strips were passively rehydrated (20°C for 12 h) and then focused (for pH 3-6: 4000V, Rapid, 11000 Vhrs; for pH 5-8: 4000V, Rapid, 9000 Vhrs) with a Protean IEF cell (Biorad). After focusing, the strips were equilibrated in DTT-containing buffer (6 M urea, 0.375 M Tris-HCL pH=8.8, 2% SDS, 20% glycerol, and 2% (w/v) DTT) for 15 minutes followed by incubation in iodoacetamide-containing buffer (6 M urea, 0.375 M Tris-HCL pH=8.8, 2% SDS, 20% glycerol, and 2.5% (w/v) iodoacetamide) for 15 minutes before rinsing briefly with standard SDS-PAGE running buffer. Molecular weight separation was achieved by running on 10% SDS-PAGE gels and visualized by silver staining. Spots of interest were extracted from the gel with a plastic pipette tip and sealed in a 1.5 ml tube. Samples were sent to Oklahoma State for MS analysis as described above.

MS statistical analysis

Statistical analysis was carried out in the freely available Perseus 1.2.0.16 software platform (https://maxquant.net/perseus/) (Tyanova et al., 2016). Label-free quantification (LFQ) intensities were imported and the raw data was filtered to remove potential contaminants or incorrect protein identifications. Expression values were

converted to $\log_2$ for data normalization before statistical analysis (Cox et al., 2014). For each biological replicate, proteins that passed the statistical threshold after being subjected to a two-sample t-test (Permutation-based FDR $p<0.05$) were kept for further analysis. Imputation was performed to replace missing values from a normal distribution. Fold change (FC) was calculated for proteins that showed statistically significant t-test differences ($p<0.05$) and threshold values $x>0.5$ (positive FC) or $x<0.5$ (negative FC). Only *Manduca* proteins that were considered statistically significant in 2 out of 3 biological replicates are present in Table S1. Principal component analysis (PCA) was performed in Perseus by selecting Analysis ➔ Clustering/PCA ➔ Principal component analysis (Benjamini-Hochberg FDR $p<0.05$).

Gene Ontology analysis

Following MS peptide identification, the protein ID corresponding to each *Manduca* hit was used to search the published protein sequence data from the *Manduca* official gene set 2. FASTA sequences were then subjected to BLAST analysis against the *Drosophila melanogaster* database at FlyBase.org using default search parameters. The resulting *Drosophila* protein names and FlyBase IDs are listed in Table S1.

***Drosophila* genetics**

All fly stocks were reared and maintained on standard cornmeal medium at 25°C. RNAi crosses were performed at 25°C. The following *Drosophila* stocks were obtained from the Bloomington (BL) *Drosophila* Stock Center (BDSC) or the Vienna *Drosophila* Resource Center (VDRC): *mef2*-Gal4 (BL27390); MHC-GFP (BL38463); UAS-*GFP RNAi* (BL9331); UAS-*DN-EcrB1* (UAS-EcR.B1-ΔC655.F645A; BL6869); UAS-*atrogin1 RNAi* (BL 31373); UAS-*tn RNAi* (v19290); UAS-*awd RNAi* (BL42532); UAS-*skap RNAi* (BL55168); UAS-*tmod RNAi* (BL31534); UAS-*Gdi RNAi* (BL 27309); UAS-*CG14207 RNAi* (BL64571); and UAS-*cib* RNAi (BL36630). A *mef2*-Gal4, MHC-GFP stock was generated using standard recombination procedures and crossed out to UAS-*cib* RNAi flies to visualize all pupal muscles.

Dissection and analysis of *Drosophila* DIOMs

To monitor DIOM atrophy, pupae were collected at 0 h, 12 h, and 24 h APF. Whole mount DIOMs were visualized and photographed using a Leica M165FC Fluorescent Stereo Microscope. Flat muscle preparations were prepared by dissection in phosphate buffered saline (PBS), followed by fixation with 4% formaldehyde in PBS for 30 min at room temperature, washed with PBS plus 0.3% Triton X and stained with Alexa Fluor™ 488 Phalloidin (Thermo Fisher Scientific) for 2 h at room temperature. Images of muscle preparations were acquired using a Zeiss LSM 700 confocal microscope, processed using the Zeiss Zen software, and assembled into figures in Photoshop Elements 12. DIOMs from the second abdominal segment (A2) were used for comparing the muscle area between the control and experimental groups. At least 6-10 flies per genotype were used to monitor DIOM development. Quantifications were performed using the 'Analyze Particles' function in Image J, and recorded in an Excel spreadsheet. The raw data was imported into GraphPad Prism 6.0 software for the generation of either bar graphs (Fig. 6A) or mean and error plots (Figs. 4D, 5C, 6D). Student t-tests followed by the Mann-Whitney tests were used to compare genotypes at each time point individually, without assuming a consistent SD. P-values and sample size are noted in each figure legend.

Quantitative PCR (qPCR)

qPCR was performed to verify RNAi knockdown. RNA was isolated from single whole wandering L3 larva using the RNeasy miniprep kit (Qiagen) in triplicate. cDNA was generated from 125 ng RNA using the SuperScript III First-Strand Synthesis System Kit (Invitrogen). Each cDNA solution was diluted 1:10 and mixed with SYBR Select Master Mix for CFX (Applied Biosystems) and the appropriate primers were added. *rp49* was used as the reference gene with the following primer sequences: forward 5′-GCCCAAGGGTATCGACAACA-3′ and reverse 5′-GCGCTTGTTCGATCCGTAAC-3′. *Atrogin* primers sequences: forward 5'-CGTTCCAAGGTGCTCGAGT-3' and reverse 5'-AACCCGGCTATCTCTCTGGT-3'. Reactions were ran on the CFX96 Touch Real-Time

PCR Detection System with CFX Manager Software (Biorad). The average of the triplicates was used to calculate the 2−ΔΔCt values (normalized fold expression) (Livak and Schmittgen, 2001).

RESULTS

The ISMs that form in the *Manduca* embryo continue to grow during the larval instar stages and undergo a 3-day period of atrophy just prior to adult eclosion, after which the ISMs undergo programmed cell death (PCD) (Schwartz and Truman, 1983). To examine the relative changes in protein abundance during this pupal phase of tissue degeneration, the ISMs from individual *Manduca* pupae were isolated at the initiation (day 15, D15) and conclusion (day 18, D18) of muscle atrophy (**Fig. 1A**). Analysis of D15 and D18 samples revealed minor differences in protein abundance visualized by SDS-PAGE electrophoresis followed by Coomassie staining (**Fig. 1B**, **asterisks**). To obtain a full profile of protein changes during the atrophy process, we utilized mass spectrometry (MS) for peptide identification. For each biological replicate at D15 or D18, samples were trypsinized, ionized by electrospray and the raw MS/MS spectra were searched against the *Manduca sexta* database (Kanost et al., 2016). Analysis of label-free quantification (LFQ) values was performed using the MaxQuant software suite to obtain a list of proteins at an FDR<0.5. A total of 244 proteins emerged from these datasets with the criteria of being present in at least two biological replicates (**Table S1**). Principal component analysis (PCA) of this core proteome set revealed biological variability between replicates, but distinct separation between D15 and D18 peptide groups (**Fig. 1C**). These findings demonstrate the high reproducibility between the developmental time points and the MS output data.

Heat map analysis was performed to evaluate expression trends during the course of ISM atrophy. Even though variability was observed between sample groups at each time point, proteins that were up- or down-regulated separated into distinct groups (**Fig. 2A**). Approximately 60.0% of the proteins identified were increased from D15 to D18 samples, while about one-third of proteins showed a decrease during this period of

atrophy (**Fig. 2B**). 4.1% of proteins were consistently detected in D15 or D18 samples, but showed variability in upregulation or downregulation and were designated 'no change.'

Distinct classes of proteins show differential changes during atrophy

To understand protein groups that are required for developmental muscle atrophy, we performed gene ontology (GO) annotation enrichment analysis. As our long-term goal is to functionally evaluate genes required for atrophy in the genetically amenable *Drosophila* model, we first used Basic Local Alignment Search Tool (BLAST) to identify *Manduca* protein orthologs in this species (**Table S1**). Approximately 1.2% (3/244) of the *Manduca* hits did not reveal a *Drosophila* counterpart using this approach. The remaining orthologous *Drosophila* proteins were then assessed for annotations based upon predicted cellular functions to uncover major descriptor terms (**Fig. 2C**). As expected, the core proteome was enriched for metabolic processes that are essential in any cellular system and highlighted by an increase in proteins that contribute to energy production, including the transport and metabolism of nucleotides, lipids, carbohydrates and amino acids. Additional categories of upregulated proteins included posttranslational modifications, chaperones, and cytoskeletal components, which will be discussed in more detail below. To validate our global MS approach, we also performed 2-dimensional gel analysis (2-D) followed by MS identification of individual protein spots. Indeed, peptide determination of 5 out of 6 individual protein spots that decreased in abundance from D15 to D18 were present in our original MS data (**Figure S1; Table S1**).

To understand specific classes of proteins that contribute to developmental muscle atrophy, we further assessed GO terms using the gene annotation and analysis resource Metascape (https://metascape.org/gp/index.html#/main/step1). Seven groups of proteins, some of which overlap, decreased in abundance from D15 to D18 (**Fig. 3A**). One class of proteins reduced in abundance comprised actin filaments and stress fibers, the latter describing contractile actin bundles usually found in non-muscle cells. Proteins that are destined for the plasma membrane, the extracellular space, or cell-cell junctions were also decreased, suggesting that intracellular modifications are prioritized over interactions with other cells or the extracellular environment.

Notably, a number of proteins that comprise contractile sarcomeres were differentially down- or up-regulated. A subset of proteins at the Z-disc decreased in abundance [*e.g.*, alpha-actinin, Zasp52, CG14207], while others showed elevated protein levels [*e.g.*, Muscle-specific protein 300 kDa (Msp300) and Muscle LIM protein at 60A (Mlp60A)]. One clear trend was the increase in A band and/or Myosin-containing proteins. Proteins of this class included Myosin heavy chain (Mhc), Myosin light chain 1 (Mlc1), Myosin light chain 2 (Mlc2), and Myofilin, among others (**Fig. 3B**). This result was somewhat surprising as the mRNA transcripts for some of these genes have previously been shown to be repressed during atrophy (Tsuji et al., 2020). Other protein groups that were broadly upregulated included proteins that comprise the endomembrane system and other cellular membranes (**Fig. 3A**). Consistent with the observed increase in proteins that influence energy production, proteins present in mitochondrial complexes, especially in the mitochondrial inner membrane, were correspondingly upregulated during atrophy.

We next examined the top 5 groups of proteins that were either down- (**Fig. 3C**) or up-regulated (**Fig. 3D**) during atrophy using Protein Analysis THrough Evolutionary Relationships (PANTHER). The largest class of reduced proteins were chaperone complexes (GO:0101031); comprised largely of seven of the eight members of the *Drosophila* chaperonin-containing T-complex (CCT1-4, CCT6-8; GO:0005832). Since CCT proteins facilitate the folding of actin and tubulin proteins, their absence further supports the observations that both of these cytoskeletal monomer subunits are decreased (**Table S1**). The second class of downregulated proteins were the larval serum complex proteins (GO:0005616). This decrease in larval serum complexes may provide an additional source of amino acids during atrophy to prevent wasteful duplication of metabolic resources (Roberts et al., 1991). Degradation of muscle tissue predicts that muscle-specific complexes will be lost. Indeed, a reduction in troponin/thin filament proteins (GO:0005861, GO:0005865), Z-disc components (GO:0030018), and actin filaments (GO:0097517, GO:0032432, GO:0005884) support this prediction. Troponins and tropomyosins are thin filament-associated proteins that bind to sarcomeric actin filaments (**Fig. 3B**). Different classes of proteins that are increased during developmental atrophy can be simplified into three main groups.

Upregulation of proteasome (GO:0000502) and peptidase complexes (GO:1905368) assure turnover of proteins to reduce muscle mass. The 20- to 40-fold increase in ATP synthase components (GO:0045255) and mitochondrial respiratory chain proteins (GO:0098803) support increased energy demands for protein turnover, in addition to providing ribosomal subunits (GO:0005840) for protein translation, suggesting that atrophy requires a substantial shift in energy metabolism to promote muscle catabolism.

Drosophila DIOMs as a model for muscle atrophy

Holometabolous insects make two sets of muscles during their life cycles, one in embryogenesis for larval movement and the other during pupation for adult life (Bothe and Baylies, 2016). During metamorphosis, remodeling of the larval musculature assures muscles are functional for post-emergent functions, including walking, mating, and flight. While the *Manduca* ISMs are ideal for biochemical studies, this organism lacks the ability for routine targeted genetic manipulations, such as RNA interference (RNAi) to assess protein function (Garbutt et al., 2013). To functionally test the validity of our MS dataset and to directly compare conserved roles for proteins in developmental muscle atrophy across species, we chose to examine muscle remodeling during *Drosophila* pupation.

Two groups of muscles that undergo morphogenesis during the *Drosophila* pupal transition are the dorsal external oblique muscles (DEOMs) and the dorsal internal oblique muscles (DIOMs) (Kuleesha et al., 2016a; Kuleesha et al., 2016b; Wasser et al., 2007; Zirin et al., 2013). Both of these muscle groups are present in abdominal segments A1 to A7 and can be visualized with a Myosin heavy chain (MHC)-GFP transgene (**Fig. 4A**). The DEOMs are subject to histolysis and degenerate between 12-24 h after puparium formation (APF) depending on their anatomical location (**Figs. 4A,B**). In contrast, the DIOMs undergo two distinct phases: a period of atrophy followed by hypertrophy in the second half of pupation before adult eclosion. While the entire period of atrophy continues until ~50 h APF, the reduction in muscle area is readily apparent by 24 h APF and was thus used as an endpoint to assess the presence or absence of normal atrophy (**Figs. 4A,B**). In vivo analysis of *GFP RNAi* control muscles labeled with phalloidin showed a ~40% or 70% decrease in muscle area by 12 h and 24 h, respectively (**Figs. 4C,D**). Since ecdysone regulates remodeling of the *Manduca*

dorsal external oblique body wall muscles (Hegstrom et al., 1998), we first tested whether muscle expression of a dominant-negative ecdysone receptor (*mef2>DN-EcR*) prevents DIOM degeneration. Consistent with Zirin, et al. (Zirin et al., 2013), we confirmed the persistence of the DIOMs at both 12 h and 24 h APF (**Figs. 4C,D**). These data validate the *Drosophila* DIOMs as a genetic model to verify hits obtained in our *Manduca* MS dataset.

Upregulation of protein degradation components

Elevated protein turnover is a conserved hallmark of muscle atrophy (Bilodeau et al., 2016; Khalil, 2018; Kitajima et al., 2020). As shown in **Fig. 3D**, protein subunits that comprise the proteasome were the most over-represented as atrophy progressed. We mapped the proteins in the 'Proteasome regulatory' and 'Peptidase' complexes using the STRING (https://string-db.org/) and Cytoscape (https://cytoscape.org/) software programs (**Fig. 5A, Table S1**). The resulting protein interaction network revealed coordinate upregulation of proteasomal proteins (light blue boxes) that physically interact with deubiquitinating enzymes (DUBs) (yellow ovals) and peptidases (light purple ovals). DUBs typically remove ubiquitin (Ub) independent of, or in conjunction with, proteasomal proteolysis (Dikic, 2017). Ubiquitin-specific protease 14 (Usp14) reversibly associates with the 19S component of the proteasome (Wertz and Murray, 2019); reflected in our interactome data as a protein that links other DUBs, including Ubiquitin carboxy-terminal hydrolase (Uch), Ubiquitin-specific protease 5 (Usp5), and Ubiquitin-specific protease 7 (Usp7), to the proteasome. 29 out of 33 proteasome subunits were enriched after the onset of atrophy, with their relative locations within the proteasome shown in **Fig. 5B**. Each α or β subunit of the 20S core particle (CP) possesses catalytic activity for substrate degradation, while subunits that comprise the regulatory particles (RP), including the Regulatory particle triple-A ATPases (Rpt 1-6) or Regulatory particle non-ATPases (Rpn 1-15), assists in the recognition and unfolding of client proteins (Tanaka, 2009). These data confirm the overall sensitivity of the MS approach, as over 87% of the expected proteasome components were identified as having altered protein levels during atrophy.

E3 ubiquitin ligase proteins append K48-linked Ub chains to proteins destined for proteasomal turnover. Three E3 proteins have been extensively studied in mammalian muscle atrophy: Muscle RING-finger 1 (MuRF1), Atrogin-1/MAFbx, and Tripartite motif-containing protein 32 (TRIM32). Protein levels of MuRF1 and Atrogin-1 are rapidly induced in all types of atrophy (Bodine and Baehr, 2014; Gomes et al., 2001), while TRIM32 functions during atrophy upon fasting (Cohen et al., 2012). Since none of these proteins, nor any other E3 ligases, were upregulated in our experimental conditions during *Manduca* atrophy, we wondered if this organism possesses homologous proteins. Indeed, BLAST searches of the corresponding mammalian protein sequences revealed modest sequence similarities to proteins present in both *M. sexta* and *D. melanogaster*. TRIM9, the protein with the most identity to MuRF1 (*M. sexta* - 20.67%; *D. melanogaster* - 21.65%), is highly expressed in the *Drosophila* nervous system (Morikawa et al., 2011; Song et al., 2011). In contrast, publications by us and others have shown that both *Drosophila* Atrogin-1/CG11658 and TRIM32 [encoded by *thin* (*tn*)] are enriched in muscle tissue (Bawa et al., 2020; Domsch et al., 2013; LaBeau-DiMenna et al., 2012; Vishal et al., 2018). Muscle knockdown of either *atrogin-1* or *tn mRNA* transcripts both show a partial block of DIOM degeneration (**Fig. 5C; Figure S2**). It is not clear why these proteins were not detected in the *Manduca* MS dataset as we identified a clear orthologous protein for both Atrogin-1/F-box only protein 32 (**Fig. 5D**) and TRIM32 (**Fig. 5E**) in both *Drosophila* and *Manduca*. Moreover, *Manduca* possesses two isoforms of each protein, each of which is slightly more closely related to their mammalian counterparts than the *Drosophila* proteins. These results together convincingly support a role for proteasome components, DUBs, and E3 ligase proteins required for increased protein turnover during muscle atrophy.

Actin filament proteins are differentially regulated during atrophy

Next we wanted to assess if the *Drosophila* DIOM system could be a good experimental model to validate proteins that were either up- or down-regulated during *Manduca* atrophy. Six genes for which we could obtain RNAi lines were tested for inhibition of muscle atrophy. Knockdown of three genes, *abnormal wing discs (awd)*, *Succinyl-coenzyme A synthetase β subunit (skap)*, and *tropomodulin (tmod)*, all underwent normal DIOM atrophy similar to controls (*mef2-Gal4/+* or *mef2>GFP RNAi*) by 24 h

APF (**Fig. 6A**). In contrast, inducing RNAi against three other targets, *GDP dissociation inhibitor (Gdi)*, the chaperone *CG14207*, or *ciboulot (cib),* blocked DIOM atrophy to different extents (**Fig. 6A**).

Proteins that comprise the thin filament and/or interact with actin are predominantly downregulated from D15 to D18 (**Figs. 3A,C**). Exceptions include proteins that negatively regulate actin filament formation (Gelsolin, Cofilin, and Capulet/CAP), which would be expected to increase if destruction of actin filaments is essential for sarcomere breakdown. Mapping the actin interactome using STRING and Cytoscape revealed three distinct clusters of proteins (**Fig. 6B**). The multiprotein complex Chaperone Containing TCP-1 (CCT) consists of 8 subunits, 7 of which are represented in the MS data. Downregulation of Act57B, Act88F, αTub84D, and βTub56D in addition to the CCT complex is consistent with a major role for this molecular chaperone in assisting with the folding of newly synthesized actin and tubulin subunits, although it is likely that other substrates exist.

The largest group that forms the core of the actin interactome network are proteins that are part of, or associated with, actin thin filaments. Act57B and Act88F are muscle actin proteins predominate in *Drosophila* larval and pupal muscles (Fyrberg et al., 1980; Tobin et al., 1980). Actin-binding proteins, including Tropomyosin 1, Tropomyosin 2, Troponin C at 25D, Troponin C at 73F, and tropomodulin, all decrease in abundance from D15 to D18. Since blocking Cib function qualitatively showed the strongest phenotype (**Fig. 6A**) and was reduced in our label-free (**Table S1**) and 2-D gel (**Figure S1**) MS experiments, we chose to examine this further. Cib has sequence similarity similar to mammalian β-thymosin. While β-thymosin binds to G-actin to sequester monomer addition, Cib functionally behaves like Profilin to promote growth at barbed, but not pointed ends, of actin filaments during *Drosophila* brain metamorphosis (Boquet et al., 2000). To functionally test the requirement for Cib in DIOM atrophy, we again employed RNAi knockdown during pupal development. Compared to control *GFP RNAi* muscles, knockdown of Cib prevented muscle atrophy, not only in the abdominal segment shown (**Fig. 6C**, middle panel), but in the DIOMs of all segments (**Fig. 6D,** bottom panel; compare to **Fig. 4A**). These data together solidify for the first time a functional role for Cib in muscle remodeling during metamorphosis.

DISCUSSION

The large size of insect ISMs provide a distinctive advantage in garnering enough material for biochemical analyses and subsequent protein identification using MS. Indeed, a previous study uncovered 15 proteins using 2D gel electrophoresis that showed differential expression of skeletal muscle proteins in the silkworm *Bombyx mori* from the last day of larval development compared to the end of pupal metamorphosis (Zhang et al., 2007). Here, we expand upon these previous findings to directly assess overall protein composition distinctly during the period of muscle atrophy in the ISMs. Our conservative estimation predicts that <3% of proteins show increased or decreased protein levels to ensure tight regulation of developmental atrophy. More importantly, these findings highlight conserved aspects of atrophy across Lepidopteran and Dipteran insects.

RNA vs protein levels

Most of the published *Manduca* ISM studies have examined mRNA levels as a readout during atrophy (Haas et al., 1995; Hu et al., 1999; Schwartz et al., 1990; Sun et al., 1996), including a recent comprehensive study examining differential gene expression during skeletal muscle atrophy (Tsuji et al., 2020). Here we examine global changes in the skeletal muscle proteome, thus providing an opportunity to compare relative transcript and corresponding protein levels. Clear similarities were obvious in both datasets, including a decrease in components that positively regulate actin filament assembly and actin-mediated cell contraction. Similar upregulated RNA and protein levels were observed with proteasome components and some elements of metabolic activity, including catalytic and transport activity. More surprising were notable differences between transcript and protein levels for myosin and other thick filament proteins. For example, *Mhc* and *Mlc1* mRNA levels have been shown to decrease during developmental muscle atrophy (Tsuji et al., 2020), while we observed an increase in both Mhc and Mlc1 protein levels, along with other thick filament-associated proteins (Myofilin, Flightin).

Multiple explanations may account for the preferential loss of thin filament proteins and concomitant enrichment of thick filament proteins during atrophy. Foremost, the relative half-lives for major contractile proteins may differ. If both genes are

transcriptionally repressed, but Mhc has a longer half-life than actin, it may appear that Mhc protein abundance is higher. Alternatively, increased protein stability may reflect a biological necessity to undergo ordered destruction of the sarcomere. Myosin binding protein-C (MyBP-C), Myosin light chains 1 and 2 (MyLC1 and MyLC2) are important for thick filament stability and their selective loss during atrophy precedes degradation of mammalian Myosin heavy chain (MyHC) (Cohen et al., 2009). Thus, the elevated levels of Mlc1 and other thick filaments proteins may serve to delay Mhc protein degradation. Tight regulation of sarcomere breakdown is consistent with opposing changes in the levels of proteins that either comprise or regulate thin filament homeostasis. Monomeric actin subunits (Act57B, Act88F), actin folding chaperones (CCTs) or thin filament-associated proteins (tmod, Tm1, Tm2) are reduced in protein abundance. In contrast, elevated levels of the actin filament depolymerizing factors Cap/CAP and Tsr/Cofilin ensure disassembly of the thin filament, independent of thick filament dynamics.

Supported by these observations, we postulate a model whereby ordered, sequential steps lead to myofibril breakdown. In this model, disassembly of the thin filament precedes the destruction of thick filament proteins. It is likely that accessory proteins, such as ubiquitin ligases, proteases, and/or chaperones may facilitate the removal of proteins from intact myofibrils for subsequent degradation (Aweida and Cohen, 2021). Our data shows upregulation of a number of putative proteases (Dipeptidyl aminopeptidase III, tripeptidyl-peptidase II, Puromycin sensitive aminopeptidase) and Valosin-containing protein (VCP)/p97, an ATPase complex that is required during mammalian muscle atrophy for the accelerated degradation of muscle substrates (Piccirillo and Goldberg, 2012). It would be valuable to extend the genetic analysis in the *Drosophila* DIOM model to further examine the temporal and spatial contribution of thick filament, thin filament, additional chaperone proteins (CTT1-4,6-8, l(2)efl/CryAB, Hsp60A, etc.) to further define our atrophy model.

Atrophy in insects vs mammals

Mammalian skeletal muscle atrophy is triggered by numerous, diverse pathological conditions, including renal failure, diabetes, sepsis, and cancer cachexia (Cohen et al., 2015; Ebert et al., 2019; Gao et al., 2018; Piccirillo et al., 2014). Normally required to

maintain the balance between anabolic and catabolic pathways, elevated levels of pro-inflammatory cytokines, such as Tumor Necrosis Factor-α (TNF-α), Interleukin (IL)-1, IL-6, and myostatin, leads to the destructive breakdown of skeletal muscle proteins. Multiple studies support a role for the mammalian steroid hormone glucocorticoid as a general mediator of muscle wasting in multiple disease states to promote muscle protein breakdown (Braun and Marks, 2015; Menconi et al., 2007; Schakman et al., 2008). Structurally similar to glucocorticoids, the arthropod steroid hormone ecdysone developmentally regulates muscle atrophy (Hegstrom et al., 1998; Schwartz and Truman, 1982; Zirin et al., 2013). An additional shared feature between developmental atrophy and glucocorticoid-induced mammalian muscle atrophy is that loss of muscle mass does not affect normal physiological properties such as tetanic contractions, excitation-contraction coupling, or the amount of force generated per cross-sectional area (Laszewski and Ruff, 1985; Ruff et al., 1982; Schwartz and Ruff, 2002).

Two evolutionarily conserved biological processes that control the degradation of cellular material during muscle atrophy are the ubiquitin–proteasome system (UPS) and the autophagy-lysosome system (ALS) (Bonaldo and Sandri, 2013; Dikic, 2017; Khalil, 2018; Kitajima et al., 2020). Many genes that comprise the UPS or ALS are classified as so-called atrogenes and are upregulated in various catabolic conditions (Taillandier and Polge, 2019). Blocking the UPS in numerous mammalian studies reduces muscle atrophy associated with pathological conditions (Kandarian and Jackman, 2006; Tawa et al., 1997). The atrogenes MurF1 and Atrogin-1/MAFbx were the first two muscle-specific ubiquitin E3 ligases to be discovered that are upregulated in nearly all catabolic conditions tested thus far (Bodine and Baehr, 2014; Gomes et al., 2001). Additional E3 ligases, including TRIM 32, Cbl-b, TRAF6, and UBR4, also play essential roles in the prevention of muscle wasting (Cohen et al., 2012; Nakao et al., 2009; Paul et al., 2010). Like mammals, developmental atrophy in insects is associated with upregulation of all the components of UPS system (Dawson et al., 1995; Haas et al., 1995; Haas et al., 2007; Hastings et al., 1999; Jones et al., 1995; Löw et al., 1997; Schwartz et al., 1990). Here we confirm that the Atrogin-1 and Trim32 E3 ubiquitin ligases play a similar role in regulating developmental atrophy. Since one of the major ubiquitin ligases, MurF1, is missing in the insect system (Piccirillo et al., 2013), there may be other novel proteins that replace MurF1 function during developmental atrophy.

Both TRIM32 and TRAF6 have been recently linked to autophagy through regulation of Unc-51 like autophagy activating kinase (ULK1)/Autophagy related 1 (ATG1) (Di Rienzo et al., 2019; Paul et al., 2012), part of a complex that initiates autophagy (Dikic, 2017). Additional FOXO-mediated atrogenes that regulate autophagy during muscle atrophy include Cathepsin L, LC3, and GabarapL1 (Lecker et al., 2004; Zhao et al., 2007). Similarly, developmental atrophy in *Manduca* is marked by a severe increase in the number of both lysosomes and autophagic vesicles (Beaulaton and Lockshin, 1977; Schwartz, 2008). This functional requirement has been substantiated in the *Drosophila* DIOMs, whereby blocking the function of five different autophagy-related genes, *Atg5, Atg9, Atg12, Atg17* and *Atg18* reduced developmental muscle atrophy (Kuleesha et al., 2016a). Although, mammalian and insect studies have highlighted the importance of autophagy/lysosomal pathway in muscle atrophy, there are still a lot of unanswered questions to further understand the connection between the UPS and the ALS. The DIOMs provide an excellent model for further genetic analysis and/or to perform suppressor/enhancer screens to identify new components that contribute to muscle atrophy. It would also be interesting to test if actin regulatory proteins, such as Cib, play a role in mammalian atrophy.

Limitations of the current approach

The global MS approach we undertook in this manuscript did not assay for post-translational modifications. Thus, it is possible that altered protein functions (*e.g.,* phosphorylation, ubiquitination, etc.), without changes in overall protein levels, were not detected. Another limitation was analysis of only two timepoints at D15 and D18. Timepoints subjected to high resolution RNAseq by the Schwartz group were collected each day of *Manduca* pupal development, from day 13 to day 18 and thus provide a more comprehensive view of gene regulation during initiation, progression, and the conclusion of atrophy (Tsuji et al., 2020). In the wild, *Manduca* pupate in the ground and their circadian clock in entrained by temperature. It is possible that the 12:12 photoperiod and constant temperature used for developmental coordination in the laboratory setting contributed to individual variability observed among biological replicates. An additional caveat is over interpreting the present MS data to make

conclusions about the relative classes of protein that are up- or downregulated. For example, if the contractile proteins are preferentially degraded during atrophy and the same mass of ISM tissue is present in each experiment, there could be an automatic enrichment of cytoplasmic and/or nuclear proteins as well as components of the endomembrane system.

In conclusion, work presented here further highlights some parallels between developmental atrophy in insects and diseased induced mammalian atrophy. Thus, a combination of studies in *Manduca* and *Drosophila* will provide valuable insights for understanding the mechanism regulating muscle atrophy in mammals.

ACKNOWLEDGEMENTS

A special thank you to Mike Kanost for providing *Manduca* specimens and to Lisa Brummet for assistance with *Manduca* pupal staging. Thank you to Dr. Steve Hartson and Janet Rogers at the Recombinant DNA/Protein Resource Facility at Oklahoma State University for technical advice and assistance with the MS experiments. We are grateful to the BDSC (https://bdsc.indiana.edu/) and VDRC (www.vdrc.at) for providing fly stocks. The BDSC is supported by a grant from the Office of the Director of the National Institutes of Health under Award Number P40OD018537.

COMPETING INTERESTS

The authors have declared that no competing interests exist.

FUNDING

Research reported in this publication was supported by the National Institute of Arthritis and Musculoskeletal and Skin Disease (NIAMS) of the National Institutes of Health under award 2R01AR060788 to E.R.G. Portions of this work were also supported by the USDA National Institute of Food and Agriculture, Hatch-Multistate project 1024217.

REFERENCES

Aweida, D. and Cohen, S. (2021). Breakdown of Filamentous Myofibrils by the UPS-Step by Step. *Biomolecules* **11**.

Bawa, S., Gameros, S., Baumann, K., Brooks, D. S., Kollhoff, J. A., Zolkiewski, M., David Re Cecconi, A., Panini, N., Russo, M., Piccirillo, R. et al. (2020). Costameric Integrin and Sarcoglycan protein levels are altered in a. *Mol Biol Cell*, mbcE20070453.

Bayline, R. J., Dean, D. M. and Booker, R. (2005). Inhibitors of ubiquitin-dependent proteolysis can delay programmed cell death of adult intersegmental muscles in the moth Manduca sexta. *Dev Dyn* **233**, 445-55.

Beaulaton, J. and Lockshin, R. A. (1977). Ultrastructural study of the normal degeneration of the intersegmental muscles of Anthereae polyphemus and Manduca sexta (Insecta, Lepidoptera) with particular reference of cellular autophagy. *J Morphol* **154**, 39-57.

Bilodeau, P. A., Coyne, E. S. and Wing, S. S. (2016). The ubiquitin proteasome system in atrophying skeletal muscle: roles and regulation. *Am J Physiol Cell Physiol* **311**, C392-403.

Bodine, S. C. and Baehr, L. M. (2014). Skeletal muscle atrophy and the E3 ubiquitin ligases MuRF1 and MAFbx/atrogin-1. *Am J Physiol Endocrinol Metab* **307**, E469-84.

Bonaldo, P. and Sandri, M. (2013). Cellular and molecular mechanisms of muscle atrophy. *Dis Model Mech* **6**, 25-39.

Boquet, I., Boujemaa, R., Carlier, M. F. and Préat, T. (2000). Ciboulot regulates actin assembly during Drosophila brain metamorphosis. *Cell* **102**, 797-808.

Bothe, I. and Baylies, M. K. (2016). Drosophila myogenesis. *Curr Biol* **26**, R786-91.

Braun, T. P. and Marks, D. L. (2015). The regulation of muscle mass by endogenous glucocorticoids. *Front Physiol* **6**, 12.

Cohen, S., Brault, J. J., Gygi, S. P., Glass, D. J., Valenzuela, D. M., Gartner, C., Latres, E. and Goldberg, A. L. (2009). During muscle atrophy, thick, but not thin, filament components are degraded by MuRF1-dependent ubiquitylation. *J Cell Biol* **185**, 1083-95.

Cohen, S., Nathan, J. A. and Goldberg, A. L. (2015). Muscle wasting in disease: molecular mechanisms and promising therapies. *Nat Rev Drug Discov* **14**, 58-74.

Cohen, S., Zhai, B., Gygi, S. P. and Goldberg, A. L. (2012). Ubiquitylation by Trim32 causes coupled loss of desmin, Z-bands, and thin filaments in muscle atrophy. *J Cell Biol* **198**, 575-89.

Cox, J., Hein, M. Y., Luber, C. A., Paron, I., Nagaraj, N. and Mann, M. (2014). Accurate proteome-wide label-free quantification by delayed normalization and maximal peptide ratio extraction, termed MaxLFQ. *Mol Cell Proteomics* **13**, 2513-26.

Cox, J. and Mann, M. (2008). MaxQuant enables high peptide identification rates, individualized p.p.b.-range mass accuracies and proteome-wide protein quantification. *Nat Biotechnol* **26**, 1367-72.

Dawson, S. P., Arnold, J. E., Mayer, N. J., Reynolds, S. E., Billett, M. A., Gordon, C., Colleaux, L., Kloetzel, P. M., Tanaka, K. and Mayer, R. J. (1995). Developmental changes of the 26 S proteasome in abdominal intersegmental muscles of Manduca sexta during programmed cell death. *J Biol Chem* **270**, 1850-8.

Di Rienzo, M., Antonioli, M., Fusco, C., Liu, Y., Mari, M., Orhon, I., Refolo, G., Germani, F., Corazzari, M., Romagnoli, A. et al. (2019). Autophagy induction in atrophic muscle cells requires ULK1 activation by TRIM32 through unanchored K63-linked polyubiquitin chains. *Sci Adv* **5**, eaau8857.

Dikic, I. (2017). Proteasomal and Autophagic Degradation Systems. *Annu Rev Biochem* **86**, 193-224.

Domsch, K., Ezzeddine, N. and Nguyen, H. T. (2013). Abba is an essential TRIM/RBCC protein to maintain the integrity of sarcomeric cytoarchitecture. *J Cell Sci* **126**, 3314-23.

Ebert, S. M., Al-Zougbi, A., Bodine, S. C. and Adams, C. M. (2019). Skeletal Muscle Atrophy: Discovery of Mechanisms and Potential Therapies. *Physiology (Bethesda)* **34**, 232-239.

Fyrberg, E. A., Kindle, K. L. and Davidson, N. (1980). The actin genes of Drosophila: a dispersed multigene family. *Cell* **19**, 365-78.

Gao, Y., Arfat, Y., Wang, H. and Goswami, N. (2018). Muscle Atrophy Induced by Mechanical Unloading: Mechanisms and Potential Countermeasures. *Front Physiol* **9**, 235.

Garbutt, J. S., Bellés, X., Richards, E. H. and Reynolds, S. E. (2013). Persistence of double-stranded RNA in insect hemolymph as a potential determiner of RNA interference success: evidence from Manduca sexta and Blattella germanica. *J Insect Physiol* **59**, 171-8.

Gomes, M. D., Lecker, S. H., Jagoe, R. T., Navon, A. and Goldberg, A. L. (2001). Atrogin-1, a muscle-specific F-box protein highly expressed during muscle atrophy. *Proc Natl Acad Sci U S A* **98**, 14440-5.

Haas, A. L., Baboshina, O., Williams, B. and Schwartz, L. M. (1995). Coordinated induction of the ubiquitin conjugation pathway accompanies the developmentally programmed death of insect skeletal muscle. *J Biol Chem* **270**, 9407-12.

Haas, K. F., Woodruff, E. and Broadie, K. (2007). Proteasome function is required to maintain muscle cellular architecture. *Biol Cell* **99**, 615-26.

Hastings, R. A., Eyheralde, I., Dawson, S. P., Walker, G., Reynolds, S. E., Billett, M. A. and Mayer, R. J. (1999). A 220-kDa activator complex of the 26 S proteasome in insects and humans. A role in type II programmed insect muscle cell death and cross-activation of proteasomes from different species. *J Biol Chem* **274**, 25691-700.

Hegstrom, C. D., Riddiford, L. M. and Truman, J. W. (1998). Steroid and neuronal regulation of ecdysone receptor expression during metamorphosis of muscle in the moth, Manduca sexta. *J Neurosci* **18**, 1786-94.

Hu, Y., Cascone, P. J., Cheng, L., Sun, D., Nambu, J. R. and Schwartz, L. M. (1999). Lepidopteran DALP, and its mammalian ortholog HIC-5, function as negative regulators of muscle differentiation. *Proc Natl Acad Sci U S A* **96**, 10218-23.

Jones, M. E., Haire, M. F., Kloetzel, P. M., Mykles, D. L. and Schwartz, L. M. (1995). Changes in the structure and function of the multicatalytic proteinase (proteasome) during programmed cell death in the intersegmental muscles of the hawkmoth, Manduca sexta. *Dev Biol* **169**, 436-47.

Kandarian, S. C. and Jackman, R. W. (2006). Intracellular signaling during skeletal muscle atrophy. *Muscle Nerve* **33**, 155-65.

Kanost, M. R. Arrese, E. L. Cao, X. Chen, Y. R. Chellapilla, S. Goldsmith, M. R. Grosse-Wilde, E. Heckel, D. G. Herndon, N. Jiang, H. et al. (2016). Multifaceted biological insights from a draft genome sequence of the tobacco hornworm moth, Manduca sexta. *Insect Biochem Mol Biol* **76**, 118-147.

Khalil, R. (2018). Ubiquitin-Proteasome Pathway and Muscle Atrophy. *Adv Exp Med Biol* **1088**, 235-248.

Kitajima, Y., Yoshioka, K. and Suzuki, N. (2020). The ubiquitin-proteasome system in regulation of the skeletal muscle homeostasis and atrophy: from basic science to disorders. *J Physiol Sci* **70**, 40.

Kuleesha, Y., Puah, W. C. and Wasser, M. (2016a). A model of muscle atrophy based on live microscopy of muscle remodelling in Drosophila metamorphosis. *R Soc Open Sci* **3**, 150517.

Kuleesha, Y., Puah, W. C. and Wasser, M. (2016b). Live imaging of muscle histolysis in Drosophila metamorphosis. *BMC Dev Biol* **16**, 12.

LaBeau-DiMenna, E. M., Clark, K. A., Bauman, K. D., Parker, D. S., Cripps, R. M. and Geisbrecht, E. R. (2012). Thin, a Trim32 ortholog, is essential for myofibril stability and is required for the integrity of the costamere in Drosophila. *Proc Natl Acad Sci U S A* **109**, 17983-8.

Laszewski, B. and Ruff, R. L. (1985). Effects of glucocorticoid treatment on excitation-contraction coupling. *Am J Physiol* **248**, E363-9.

Lecker, S. H., Jagoe, R. T., Gilbert, A., Gomes, M., Baracos, V., Bailey, J., Price, S. R., Mitch, W. E. and Goldberg, A. L. (2004). Multiple types of skeletal muscle atrophy involve a common program of changes in gene expression. *FASEB J* **18**, 39-51.

Livak, K. J. and Schmittgen, T. D. (2001). Analysis of relative gene expression data using real-time quantitative PCR and the 2(-Delta Delta C(T)) Method. *Methods* **25**, 402-8.

Löw, P., Bussell, K., Dawson, S. P., Billett, M. A., Mayer, R. J. and Reynolds, S. E. (1997). Expression of a 26S proteasome ATPase subunit, MS73, in muscles that undergo developmentally programmed cell death, and its control by ecdysteroid hormones in the insect Manduca sexta. *FEBS Lett* **400**, 345-9.

Malavaki, C. J., Sakkas, G. K., Mitrou, G. I., Kalyva, A., Stefanidis, I., Myburgh, K. H. and Karatzaferi, C. (2015). Skeletal muscle atrophy: disease-induced mechanisms may mask disuse atrophy. *J Muscle Res Cell Motil* **36**, 405-21.

Menconi, M., Fareed, M., O'Neal, P., Poylin, V., Wei, W. and Hasselgren, P. O. (2007). Role of glucocorticoids in the molecular regulation of muscle wasting. *Crit Care Med* **35**, S602-8.

Morikawa, R. K., Kanamori, T., Yasunaga, K. and Emoto, K. (2011). Different levels of the Tripartite motif protein, Anomalies in sensory axon patterning (Asap), regulate distinct axonal projections of Drosophila sensory neurons. *Proc Natl Acad Sci U S A* **108**, 19389-94.

Nakao, R., Hirasaka, K., Goto, J., Ishidoh, K., Yamada, C., Ohno, A., Okumura, Y., Nonaka, I., Yasutomo, K., Baldwin, K. M. et al. (2009). Ubiquitin ligase Cbl-b is a negative regulator for insulin-like growth factor 1 signaling during muscle atrophy caused by unloading. *Mol Cell Biol* **29**, 4798-811.

Paul, P. K., Bhatnagar, S., Mishra, V., Srivastava, S., Darnay, B. G., Choi, Y. and Kumar, A. (2012). The E3 ubiquitin ligase TRAF6 intercedes in starvation-induced skeletal muscle atrophy through multiple mechanisms. *Mol Cell Biol* **32**, 1248-59.

Paul, P. K., Gupta, S. K., Bhatnagar, S., Panguluri, S. K., Darnay, B. G., Choi, Y. and Kumar, A. (2010). Targeted ablation of TRAF6 inhibits skeletal muscle wasting in mice. *J Cell Biol* **191**, 1395-411.

Piccirillo, R., Demontis, F., Perrimon, N. and Goldberg, A. L. (2014). Mechanisms of muscle growth and atrophy in mammals and Drosophila. *Dev Dyn* **243**, 201-15.

Piccirillo, R. and Goldberg, A. L. (2012). The p97/VCP ATPase is critical in muscle atrophy and the accelerated degradation of muscle proteins. *EMBO J* **31**, 3334-50.

Roberts, D. B., Jowett, T., Hughes, J., Smith, D. F. and Glover, D. M. (1991). The major serum protein of Drosophila larvae, larval serum protein 1, is dispensable. *Eur J Biochem* **195**, 195-201.

Romanick, M., Thompson, L. V. and Brown-Borg, H. M. (2013). Murine models of atrophy, cachexia, and sarcopenia in skeletal muscle. *Biochim Biophys Acta* **1832**, 1410-20.

Ruff, R. L., Martyn, D. and Gordon, A. M. (1982). Glucocorticoid-induced atrophy is not due to impaired excitability of rat muscle. *Am J Physiol* **243**, E512-21.

Schakman, O., Gilson, H. and Thissen, J. P. (2008). Mechanisms of glucocorticoid-induced myopathy. *J Endocrinol* **197**, 1-10.

Schakman, O., Kalista, S., Barbé, C., Loumaye, A. and Thissen, J. P. (2013). Glucocorticoid-induced skeletal muscle atrophy. *Int J Biochem Cell Biol* **45**, 2163-72.

Schwartz, L. M. (2008). Atrophy and programmed cell death of skeletal muscle. *Cell Death Differ* **15**, 1163-9.

Schwartz, L. M. (2018). Skeletal Muscles Do Not Undergo Apoptosis During Either Atrophy or Programmed Cell Death-Revisiting the Myonuclear Domain Hypothesis. *Front Physiol* **9**, 1887.

Schwartz, L. M., Myer, A., Kosz, L., Engelstein, M. and Maier, C. (1990). Activation of polyubiquitin gene expression during developmentally programmed cell death. *Neuron* **5**, 411-9.

Schwartz, L. M. and Ruff, R. L. (2002). Changes in contractile properties of skeletal muscle during developmentally programmed atrophy and death. *Am J Physiol Cell Physiol* **282**, C1270-7.

Schwartz, L. M. and Truman, J. W. (1982). Peptide and steroid regulation of muscle degeneration in an insect. *Science* **215**, 1420-1.

Schwartz, L. M. and Truman, J. W. (1983). Hormonal control of rates of metamorphic development in the tobacco hornworm Manduca sexta. *Dev Biol* **99**, 103-14.

Song, S., Ge, Q., Wang, J., Chen, H., Tang, S., Bi, J., Li, X., Xie, Q. and Huang, X. (2011). TRIM-9 functions in the UNC-6/UNC-40 pathway to regulate ventral guidance. *J Genet Genomics* **38**, 1-11.

Sun, D., Sathyanarayana, U. G., Johnston, S. A. and Schwartz, L. M. (1996). A member of the phylogenetically conserved CAD family of transcriptional regulators is dramatically up-regulated during the programmed cell death of skeletal muscle in the tobacco hawkmoth Manduca sexta. *Dev Biol* **173**, 499-509.

Taillandier, D. and Polge, C. (2019). Skeletal muscle atrogenes: From rodent models to human pathologies. *Biochimie* **166**, 251-269.

Tanaka, K. (2009). The proteasome: overview of structure and functions. *Proc Jpn Acad Ser B Phys Biol Sci* **85**, 12-36.

Tawa, N. E., Odessey, R. and Goldberg, A. L. (1997). Inhibitors of the proteasome reduce the accelerated proteolysis in atrophying rat skeletal muscles. *J Clin Invest* **100**, 197-203.

Tobin, S. L., Zulauf, E., Sánchez, F., Craig, E. A. and McCarthy, B. J. (1980). Multiple actin-related sequences in the Drosophila melanogaster genome. *Cell* **19**, 121-31.

Tsuji, J., Thomson, T., Chan, E., Brown, C. K., Oppenheimer, J., Bigelow, C., Dong, X., Theurkauf, W. E., Weng, Z. and Schwartz, L. M. (2020). High-resolution analysis of differential gene expression during skeletal muscle atrophy and programmed cell death. *Physiol Genomics* **52**, 492-511.

Tyanova, S., Temu, T., Sinitcyn, P., Carlson, A., Hein, M. Y., Geiger, T., Mann, M. and Cox, J. (2016). The Perseus computational platform for comprehensive analysis of (prote)omics data. *Nat Methods* **13**, 731-40.

Vishal, K., Bawa, S., Brooks, D., Bauman, K. and Geisbrecht, E. R. (2018). Thin is required for cell death in the Drosophila abdominal muscles by targeting DIAP1. *Cell Death Dis* **9**, 740.

Voruganti, S., Kline, J. T., Balch, M. J., Rogers, J., Matts, R. L. and Hartson, S. D. (2018). Proteomic Profiling of Hsp90 Inhibitors. *Methods Mol Biol* **1709**, 139-162.

Wasser, M., Bte Osman, Z. and Chia, W. (2007). EAST and Chromator control the destruction and remodeling of muscles during Drosophila metamorphosis. *Dev Biol* **307**, 380-93.

Wertz, I. E. and Murray, J. M. (2019). Structurally-defined deubiquitinase inhibitors provide opportunities to investigate disease mechanisms. *Drug Discov Today Technol* **31**, 109-123.

Zhang, P., Aso, Y., Jikuya, H., Kusakabe, T., Lee, J. M., Kawaguchi, Y., Yamamoto, K., Banno, Y. and Fujii, H. (2007). Proteomic profiling of the silkworm skeletal muscle proteins during larval-pupal metamorphosis. *J Proteome Res* **6**, 2295-303.

Zhao, J., Brault, J. J., Schild, A., Cao, P., Sandri, M., Schiaffino, S., Lecker, S. H. and Goldberg, A. L. (2007). FoxO3 coordinately activates protein degradation by the autophagic/lysosomal and proteasomal pathways in atrophying muscle cells. *Cell Metab* **6**, 472-83.

Zirin, J., Cheng, D., Dhanyasi, N., Cho, J., Dura, J. M., Vijayraghavan, K. and Perrimon, N. (2013). Ecdysone signaling at metamorphosis triggers apoptosis of Drosophila abdominal muscles. *Dev Biol* **383**, 275-84.

Figures

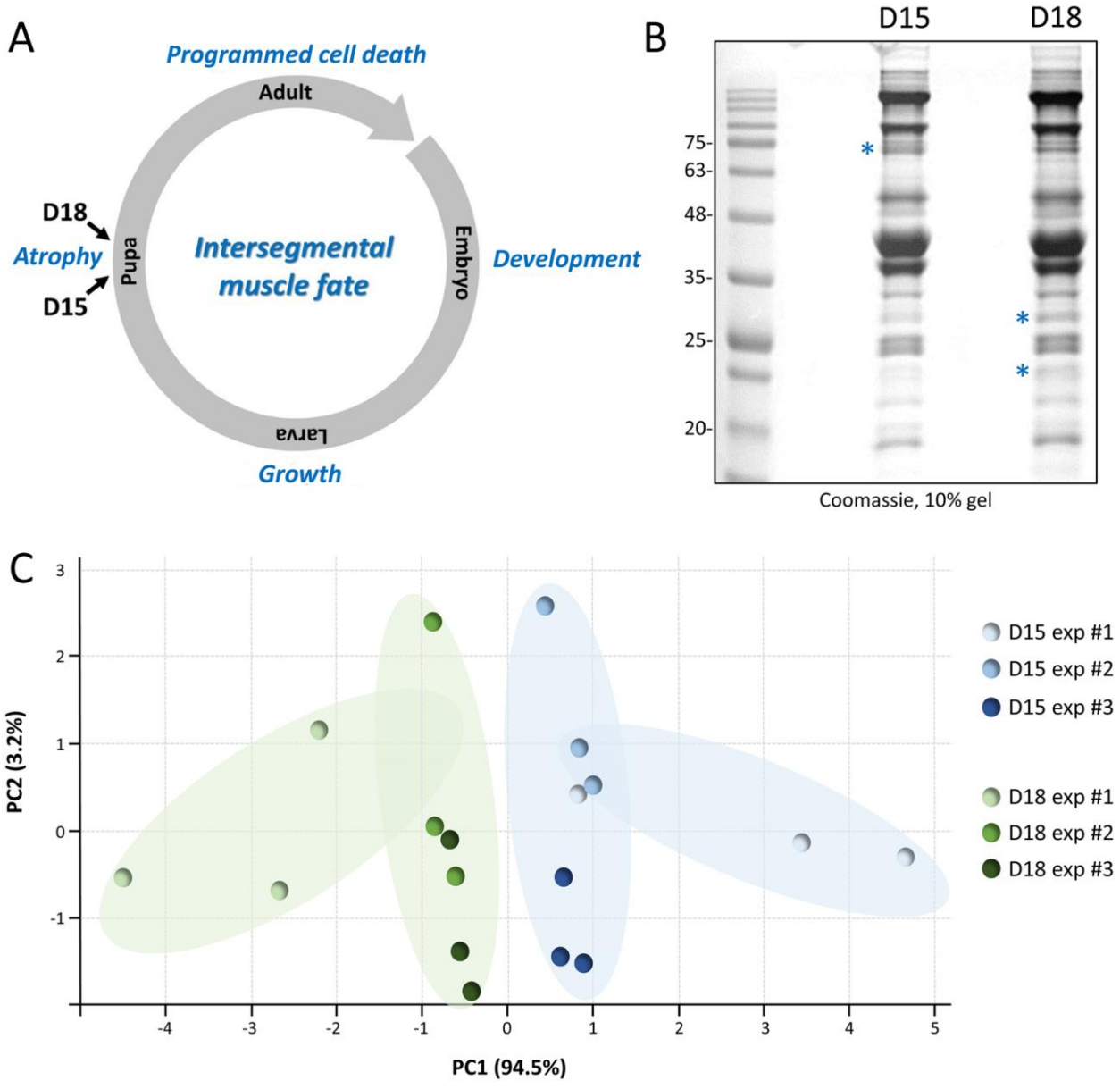

Figure 1. Experimental setup to determine the *Manduca* proteome in developmentally regulated atrophy. (A) The fate of the intersegmental muscles (ISMs) during the *Manduca sexta* life cycle. The ISMs form in embryogenesis and increase in size throughout the larval instar molts. A 3-day period of atrophy occurs between pupal D15 and D18. The ISMs eventually undergo programmed cell death after adult eclosion. (B) A representative Coomassie-stained SDS-PAGE gel with protein samples extracted at pupal D15 and D18. Obvious band intensity differences are denoted by asterisks. N=3 biological replicates. (C) Principal component analysis (PCA) reveals distinct separation between protein samples corresponding to the initiation (D15) or conclusion (D18) of developmental atrophy. The biological replicates for each time point are indicated in the same color.

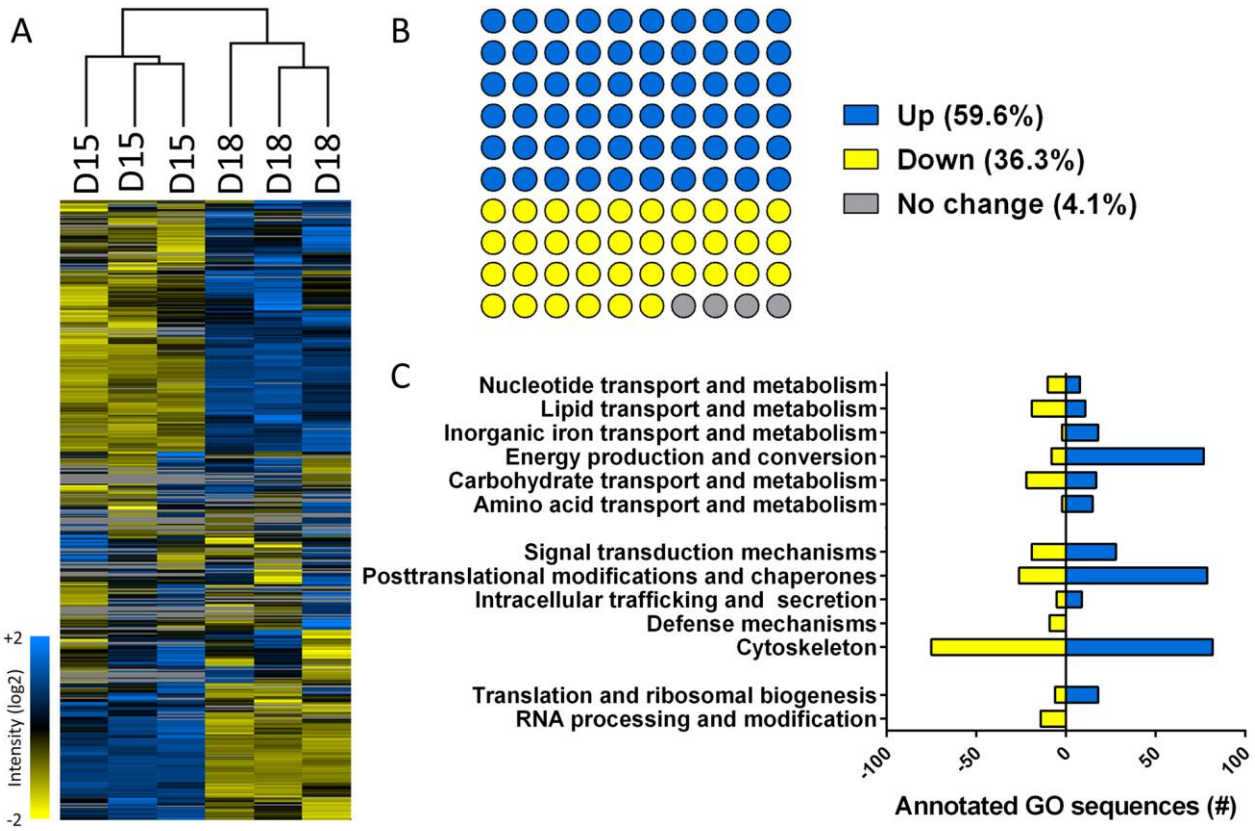

Figure 2. Global analysis of protein changes during atrophy. Upregulated proteins are shown in blue and downregulated proteins are depicted in yellow. (A) Heatmap of log_2LFQ values of individual proteins quantified during atrophy. Analysis was performed in MaxQuant. (B) Parts of whole graph depicting the total percentage of proteins changed during atrophy. The majority of proteins were increased from D15 to D18. (C) EggNOG mapping of Gene ontology (GO) terms reveal distinct classes of proteins that are upregulated or downregulated during atrophy.

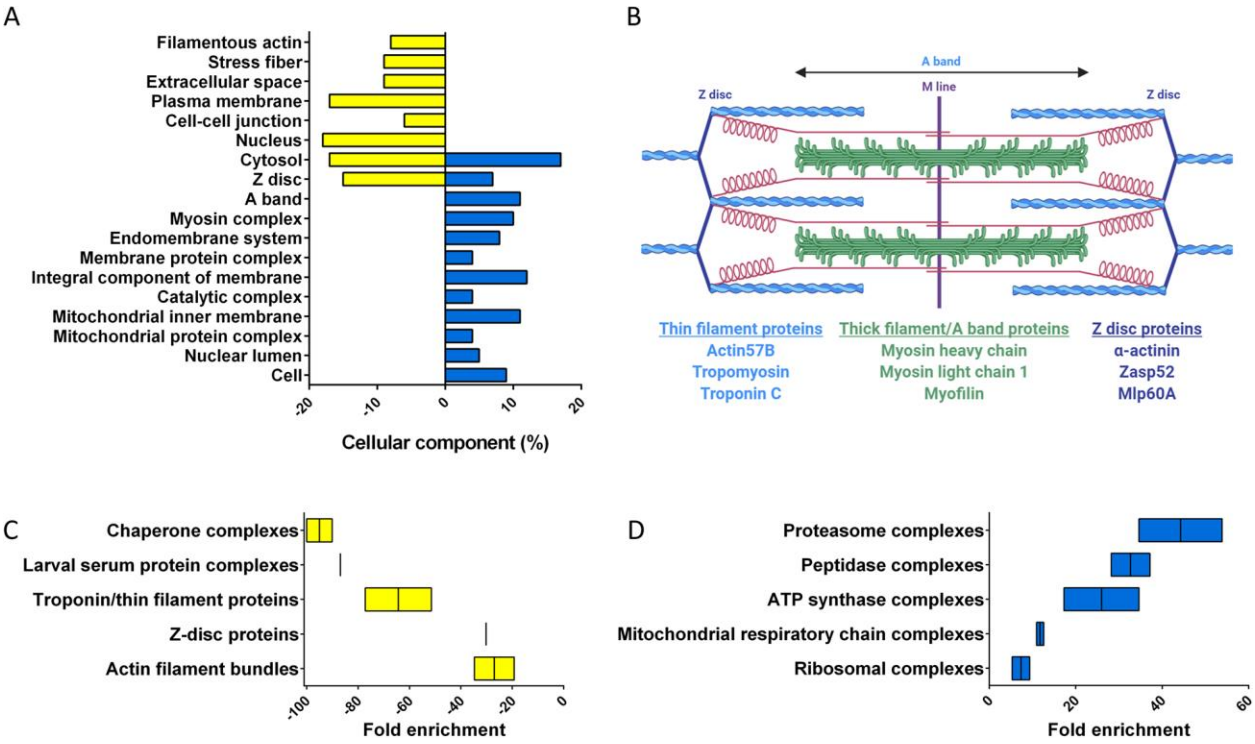

Figure 3. Cellular component analysis of up- and down-regulated proteins during atrophy. (A) Bar graph of Omicsbox classifications depicting the percentage of proteins that fall into the designated groups based upon their subcellular location. Proteins that are decreased (yellow bars) or increased (blue bars) from D15 to D18 in *Manduca*. (B) Schematic of uncontracted muscle sarcomere. Selected thin filament proteins (blue), thick filament proteins (green), and Z-disc proteins (purple) changed during atrophy are noted. (C,D) Bar graph showing the fold enrichment of distinct classes of proteins that are down-regulated (C) or up-regulated (D) using Panther GO Enrichment Analysis.

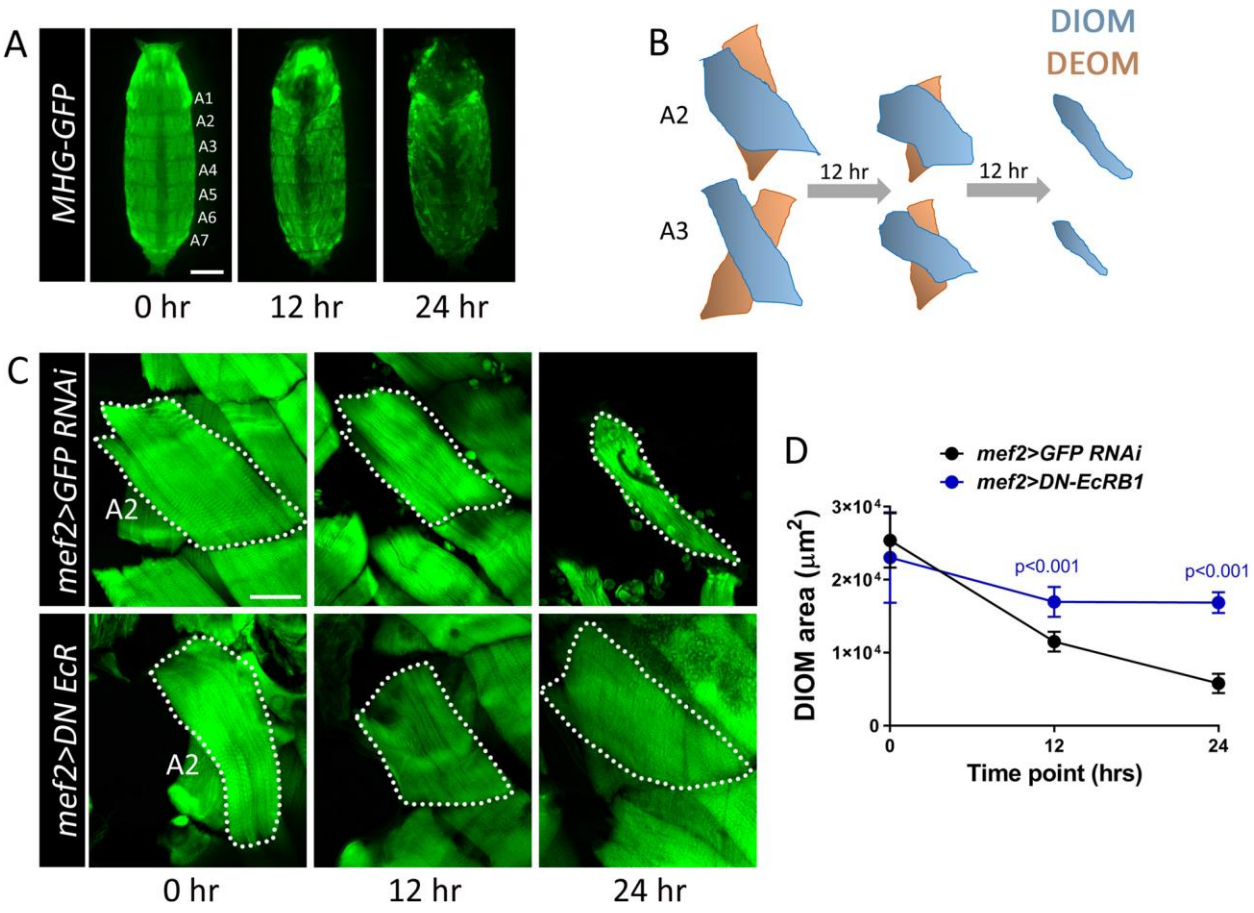

Figure 4. *Drosophila* DIOMs as a genetic model to assess developmental muscle atrophy. (A) Stereoscope view of *Drosophila* pupal development. Larval abdominal muscles at 0 h, 12 h, and 24 h APF are visualized with MHC-GFP. Scale bar, 0.5 mm (B) Schematic depicts histolysis and degeneration of the DEOMs (orange) and atrophy of the DIOMs (blue) at 0 h, 12 h, and 24 h APF. (C) Representative DIOMs from the second abdominal segment (A2) stained with phalloidin to label F-actin (white dotted lines). *UAS-GFP RNAi* under control of the *mef2*-Gal4 driver shows a consistent decrease in muscle area during the atrophic period. Muscle expression of DN-EcR prevents muscle loss. Scale bar, 50 μm (D) Grouped line plot depicting DIOM muscle area at the indicated time points. Mean +/- SD. Statistical significance determined using the Mann-Whitney test (n.s., not significant). N=7 muscles from 7 individual pupae.

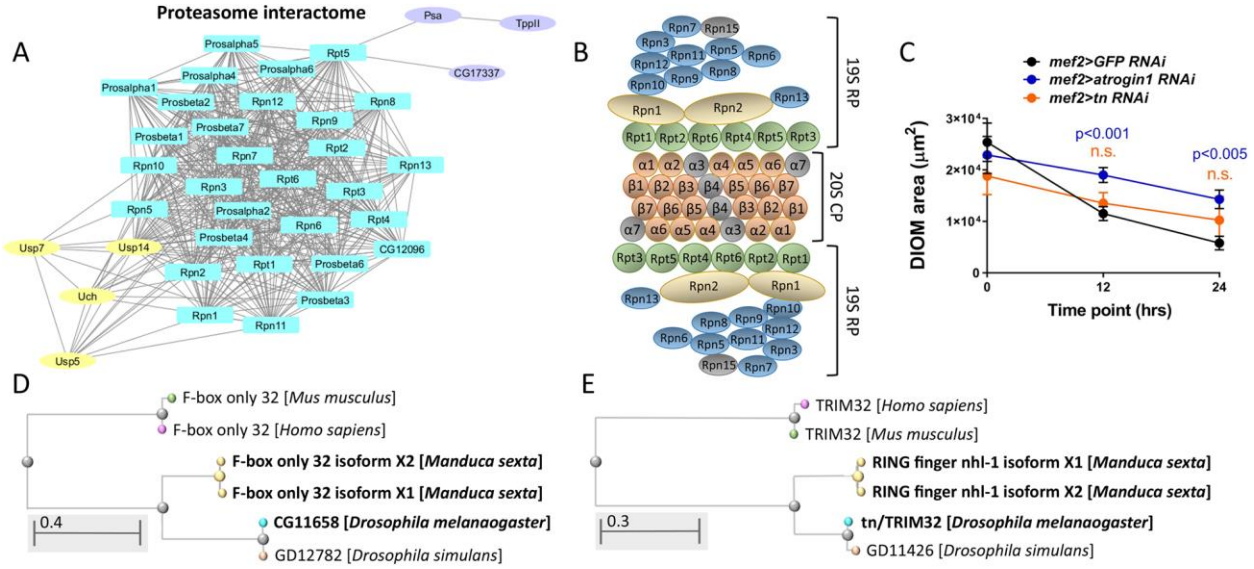

Figure 5. Proteasome components are upregulated during atrophy. (A) Cytoscape representation of the biochemical interaction networks for proteins that comprise the core particle (20S proteasome) and regulatory particle (19S) subunits (light blue). The deubiquitinating enzymes Usp5, Usp7, and Uch (light yellow) are linked to the 19S proteasome by Usp14. Other peptidases required for protein turnover that were abundantly increased are depicted in light purple or light pink. (B) Schematic drawing of proteasome subunit composition and location. Subunits in gray were not detected in our MS dataset. (C) Line plot analysis reveals that reduction of *atrogin1* (blue line) or *tn* (orange) mRNA transcripts partially block DIOM degradation. Mean +/- SD. Statistical significance determined using the Mann-Whitney test (n.s., not significant). N=7 muscles from 7 individual pupae. (D,E) Phylogenetic tree diagrams showing the evolutionary distance for F-box only 32/Atrogin1 (D) or TRIM32 (E).

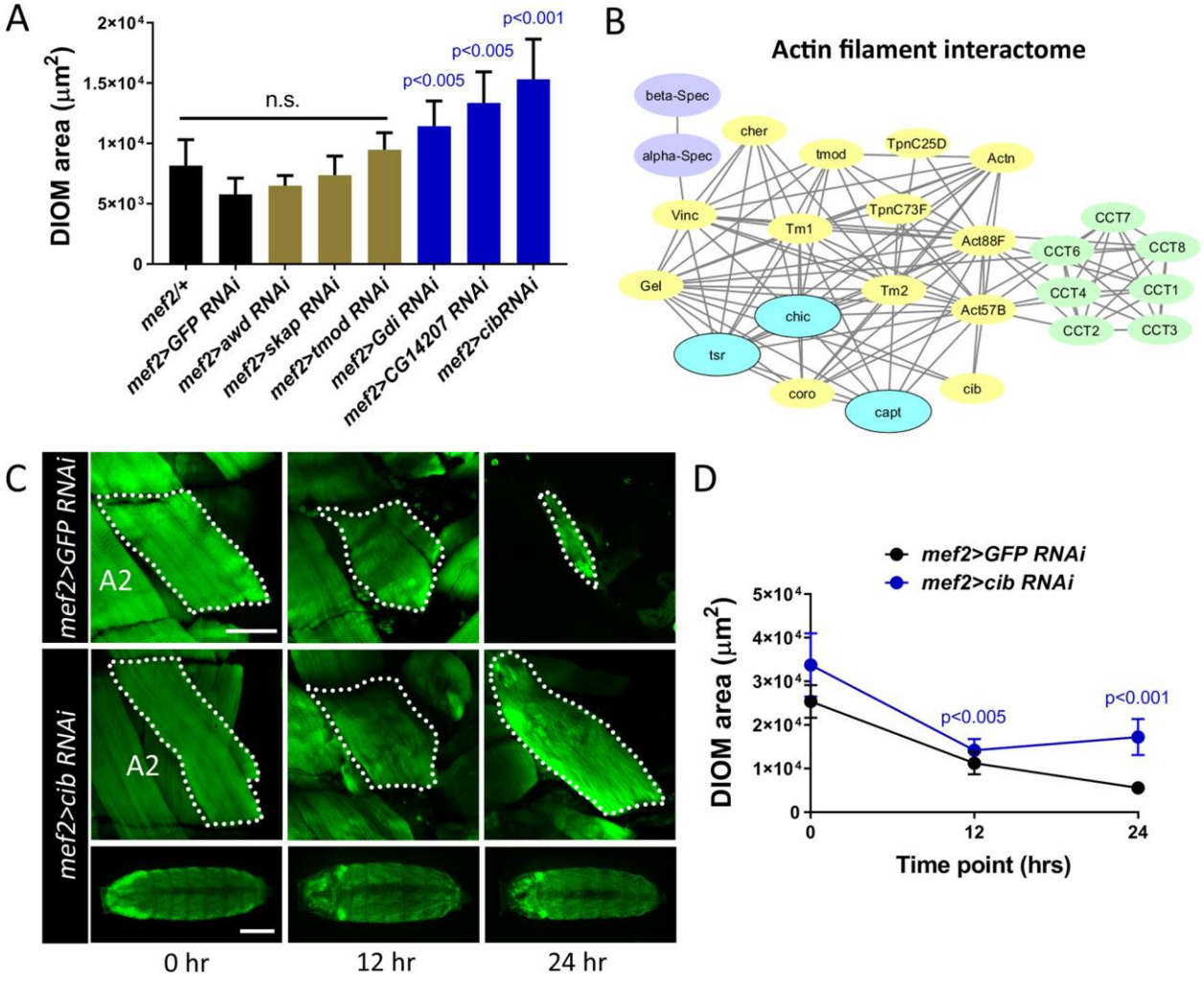

Figure 6. Cib is required to prevent atrophy. (A) Bar graph depicting the area of DIOM muscles at 24 h APF after RNAi induction of the indicated genotypes. Mean +/- SD. Statistical significance determined using one-way ANOVA with Dunn's multiple comparisons test (n.s., not significant). N≥7 muscles from 7 individual pupae. (B) Cytoscape rendering of actin, actin-binding proteins, and actin folding chaperones that form physical interactions. Proteins in yellow and green are downregulated from D15 to D18, while proteins in blue and purple are upregulated. (C) DIOMs stained with phalloidin to visualize F-actin in segment A2 (white dotted lines). Muscles expressing *GFP RNAi* undergo normal atrophy, while induction of RNAi against *cib* blocks muscle degeneration. Bottom panels depict the inability of DIOMS to undergo atrophy upon mef2>cib RNAi as assessed by an *MHC-GFP* transgene. Scale bar, 50 μm, top and middle panels; 0.5 mm, bottom panels. (D) Grouped line plot showing DIOM muscle size at 0 h, 12 h, and 24 h time points, all from individual pupae. N=6 muscles for 0 hr and N=17 for 12 h and 24 h timepoints. Mean +/- SD. Statistical significance determined using the Mann-Whitney test.

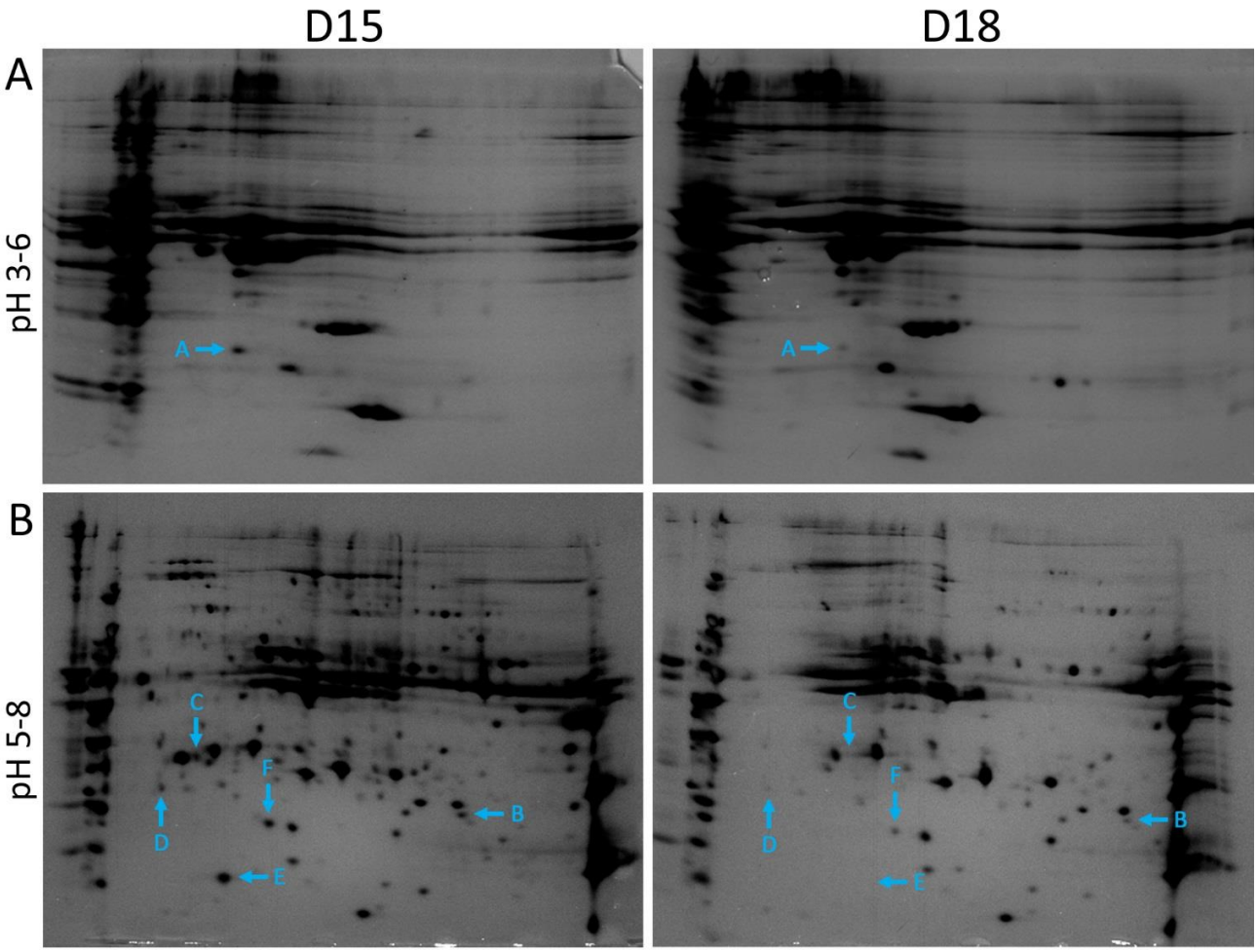

C

Spot label	*Lepidoptera* protein	Peptide coverage	*Drosophila* protein
A	LOC106104002 [*Papilio polytes*]	48%	Cib
B	KGM_12655 [*Danaus plexippus*]	10%	dj-1β
C	troponin I [*Plutella xylostella*]	19%	Troponin I (wupA)
D	unnamed protein [*Manduca sexta*]	23%	Neural Lazarillo
E	putative cuticle protein [*Manduca sexta*]	18%	no hit
F	apolipophorin III [*Manduca sexta*]	58%	LanB1

Fig. S1. 2D gel analysis reveals differential proteins changes during atrophy. (A,B) Protein lysates from D15 or D18 ISM samples were separated on SDS-PAGE gels and spots were visualized by silver staining. Spots that reveal different intensities are labeled in the pH 3- 6 (A) or pH 5-8 (B) ranges. (C) Identities of protein spots determined by MS.

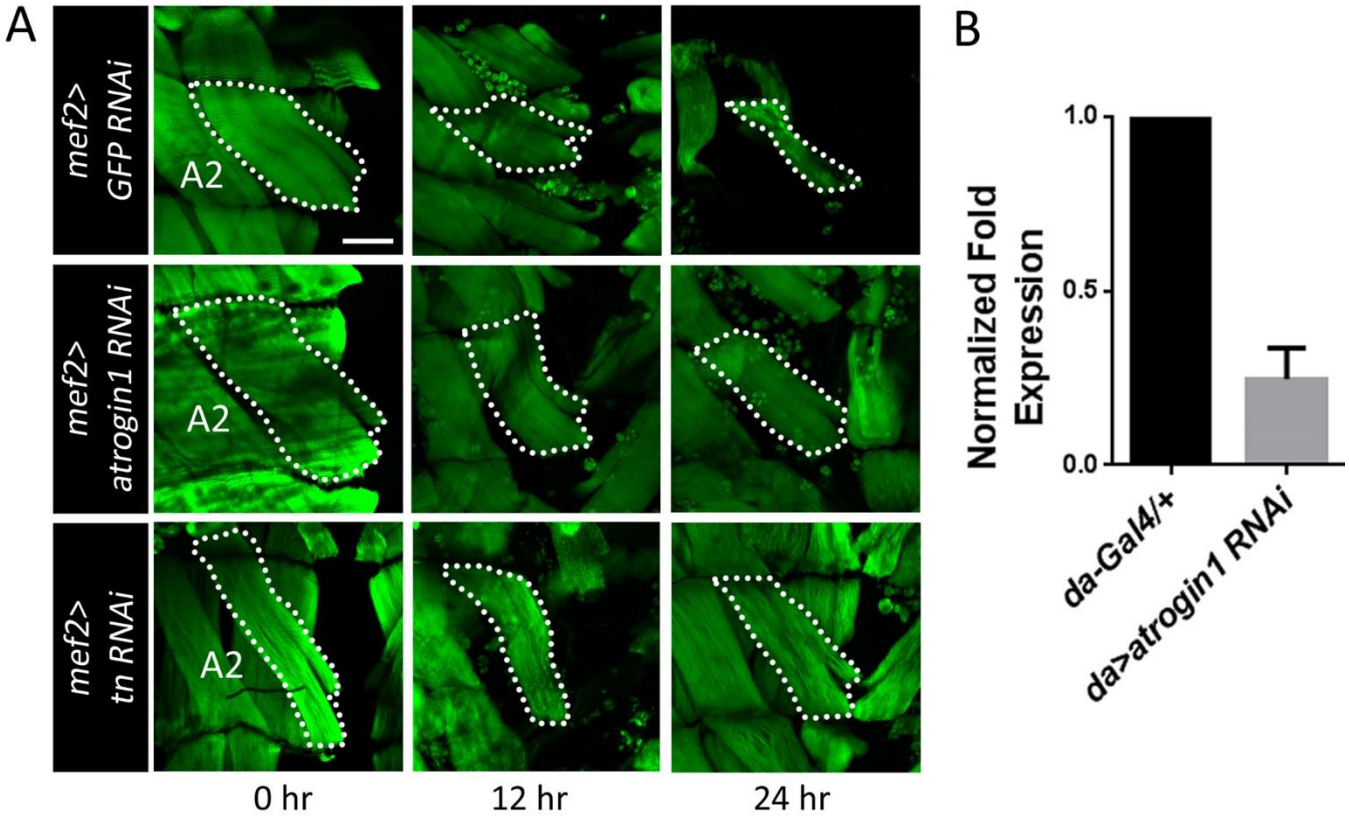

Fig. S2. Downregulation of *atrogin1* or *tn* blocks DIOM atrophy. (A) DIOMs stained with phalloidin to visualize F-actin in segment A2 (white dotted lines). Muscles expressing *GFP RNAi* undergo normal atrophy (top row). Muscle RNAi knockdown of *atrogin1* (middle row) or *tn* (bottom row) prevents a decrease in muscle size. N= 6 muscles in independent pupae. Scale bar, 50 μm (B) Bar graph showing knockdown of *atrogin1 mRNA* levels. The ubiquitous *da*-Gal4 driver is used to induce RNAi. N=3.

Table S1. *Manduca* proteins identified during developmental muscle atrophy.
(Tab 1) *Manduca* and related *Drosophila* proteins that are statistically significant ($p < 0.05$) in at least two biological replicates from D15 to D18. Proteins are listed in alphabetical order in column B. Items in bold were also identified via 2-D gel analysis. (Tab 2) Upregulated proteins sorted by average fold change in column K. (Tab 3)Downregulated proteins sorted by average fold change in column K. (Tab 4) Proteins identified that were unchanged, or were inconsistently up- or downregulated.

Click here to download Table S1